Electrochimica Acta 166 (2015) 372–384

Contents lists available at ScienceDirect

Electrochimica Acta

journal homepage: www.elsevier.com/locate/electacta

Correlation between electrochemical impedance measurements and corrosion rate of magnesium investigated by real-time hydrogen measurement and optical imaging

M. Curioni [a,*], F. Scenini [a], T. Monetta [b], F. Bellucci [b]

[a] Corrosion and Protection Centre, The University of Manchester, Manchester M13 9PL, United Kingdom
[b] University of Naples "Federico II", Department of Chemical Engineering, Materials and Industrial Production, 80125 Naples, Italy

ARTICLE INFO

Article history:
Received 31 October 2014
Received in revised form 6 March 2015
Accepted 9 March 2015
Available online 11 March 2015

Keywords:
magnesium
corrosion
electrochemical impedance spectroscopy
hydrogen collection

ABSTRACT

The corrosion behaviour of magnesium in chloride-containing aqueous environment was investigated by potentiodynamic polarization and electrochemical impedance spectroscopy (EIS) performed simultaneously with real-time hydrogen evolution measurements and optical imaging of the corroding surface. The potentiodynamic investigation revealed substantial deviations from linearity in close proximity of the corrosion potential. In particular, differences in the slope of the current/potential curves were observed for small polarizations above or below the corrosion potential. These observations, suggest that the usual method based on the use of the Stern–Geary equation to convert a value of resistance into a value of corrosion current is inadequate. Nonetheless, a very good correlation between values of resistances estimated by EIS and corrosion currents obtained from real-time hydrogen measurement was found. Real-time hydrogen measurement also enabled, for the first time, direct measurement of an 'apparent' Stern–Geary coefficient for magnesium. In order to rationalize the complex behaviours experimentally observed, an electrical model for the corroding magnesium surface is presented.

1. Introduction

The electrochemical behaviour of magnesium is relevant for a variety of applications including lightweight structures, where it determines the corrosion resistance [1–3], batteries and sacrificial anodes where it determines efficiency [4–7], and surgical implants, where it determines the rate at which the implant disappears within the human body [8,9]. The electrochemical behaviour of magnesium in aqueous environment, however, is relatively complex compared to other light metals such as aluminium or titanium. Similar to magnesium, aluminium and titanium have a large driving force for oxide formation but, unlike magnesium, the formation of a protective oxide/hydroxide layer hinders corrosion. Mg and Mg-alloys have a large thermodynamic driving force for oxide formation, since the equilibrium potential for magnesium oxidation is −2.37 V vs. SHE, but magnesium oxide/hydroxide is relatively soluble in near-neutral and acidic environment, and relatively insoluble in alkaline environment [10]. During corrosion, the increase in pH associated with hydrogen evolution stabilizes to some extent the oxide/hydroxide film.

In addition to the behaviour of the oxide, magnesium exhibits the so called 'negative difference effect' (NDE). In simple terms, the NDE relates to the increase in hydrogen evolution experimentally observed during anodic polarization and it is contrary to what would be predicted by electrochemical theory. The first interpretation of the NDE [11–13] assumes that unipolar magnesium ions are generated during anodic polarization. Once detached from the metal electrode, the unipolar magnesium ions oxidize further and reduce water, producing hydrogen gas and hydroxide ions. Thus, the NDE is considered the consequence of the increased oxidation rate of magnesium during anodic polarization that results in an increase in hydrogen evolution rate. This argument is indirectly supported by the observation that, for a value of applied anodic charge, the hydrogen evolved and the metal oxidized are in excess to those predicted by Faraday's law assuming that magnesium oxidizes in a single step to Mg^{2+}. The second interpretation of the NDE does not require assuming the existence of unipolar magnesium, and attributes the NDE to an increased cathodic activity of the magnesium surface during anodic polarization. Based the reported results from various independent approaches and on own work [14–20], the Authors' view is that the increase in

* Corresponding author.
E-mail address: michele.curioni@manchester.ac.uk (M. Curioni).

http://dx.doi.org/10.1016/j.electacta.2015.03.050

the rate of hydrogen evolution during anodic polarization is due to an increase in the cathodic activity of the regions that have undergone corrosion. Thus, by anodic polarization, corrosion propagates faster than at the free corrosion potential, generating regions with enhanced cathodic activity. The propagation of such cathodically active regions is responsible for the observed increase in hydrogen evolution during anodic polarization. Regardless of the mechanism, since the oxidation of a magnesium atom results in the generation of an hydrogen molecule, the corrosion rate of magnesium can be estimated by the hydrogen collection method [15,16,18,19,21–24].

Regardless of the exact nature of the NDE, the correlation between the data obtained by electrochemical measurement and corrosion rate requires attention, since the electrochemical response of magnesium is more complex than that observed on most other metals. Specifically, the behaviour of magnesium deviates substantially from Tafel-type kinetic due to the presence of an oxide/hydroxide layer [25] which controls the corrosion rate and due to the propagation of the cathodically active regions during anodic polarization [15,17–19,21,26]. As a consequence, extrapolation of the corrosion rates from potentiodynamic polarization curves is questionable. For similar reasons, values of resistance estimated by EIS must be used with caution, since the use of the Stern–Geary relationship is not, strictly speaking, correct.

Whereas the cathodic Tafel coefficient is generally easily obtained [21,23], the determination of the anodic Tafel coefficient is not trivial. This arises from the fact that a magnesium electrode can sustain very high anodic current with minimal anodic polarization. Such high currents are accompanied by substantial hydrogen evolution and local alkalinisation, producing a large Ohmic drop in proximity of the electrode surface. Even assuming that the anodic reaction follows Tafel behaviour, it is difficult to estimate the anodic Tafel coefficient from polarization curves not corrected for the IR drop. However, reliable correction of the IR drop is not easy, since the solution resistance (strongly affected by the presence of hydrogen bubbles) in proximity of the electrode is most likely dependent on the applied potential [17]. Generally, a well-defined and reliable linear anodic region in the Evans diagrams is not readily observed. In addition to the above issues, during impedance measurement, an inductive behaviour at the low-frequency end of the impedance spectrum is generally observed [11,21,27,28]. The physical interpretation of inductive behaviour associated to electrochemical processes is non-trivial, and that is probably the reason why this inductive behaviour is often neglected.

Apart from these 'electrical' complications, there are issues related to the practicalities during corrosion testing that might contribute to significant variations in the final result. The first issue arises from the fact that magnesium corrosion results in alkalinisation of the environment and consequent decrease in the aggressiveness of the environment if the experiment is performed in a fixed volume of electrolyte. Considering that both hydrogen measurement with the traditional method of observing visually the amount of hydrogen collected in a graduated cylinder initially filled with electrolyte and weight loss measurements require relatively long times (at least hours), it is most likely that significant differences in the environment develop during the test. As a result, the data obtained for different volumes of electrolytes and possibly different geometries of the corrosion cell might not be directly comparable.

In addition to the above, it is well known that during the early stages of corrosion the appearance of a magnesium electrode changes substantially from silvery to dark as corrosion proceeds [15,17–19,21,26]. It has been shown that such variation in appearance results in a significant difference in the cathodic potentiodynamic response, but does not produce an equally large variation in the anodic potentiodynamic response [17]. For this reason, the surface conditions prior to polarization initiation should be reported otherwise it is difficult to considered comparable the result presented in works investigating the corrosion rate on magnesium by potentiodynamic polarization [22,26,29,30]. The potential at which the polarization is initiated also has a substantial effect on the estimated corrosion rate. Specifically, considering that magnesium is more passive at high pH, when the polarization is initiated well below the corrosion potential, alkalinisation in proximity of the electrode occurs and the corrosion rate from potentiodynamic polarization is significantly underestimated [17]. On the other hand, simultaneous measurement of the cathodic potentiodynamic polarization response and hydrogen evolution, indicated that extrapolation of the linear part of the cathodic polarization curve to the open circuit potential provides a relatively accurate estimation of the corrosion current, provided that the cathodic potentiodynamic polarization is initiated at the corrosion potential [17,31].

Recently, King et al. [21] have investigated in detail the correlation between impedance measurements and corrosion rate by complementing the impedance data with weight loss and hydrogen measurement. In order to fit the impedance spectra, they used a circuit comprising an inductive part and found good correlation between the zero-frequency values of the total impedance and the corrosion rate measured by weight loss and hydrogen measurement (the term zero-frequency resistance denotes in this work the equivalent resistance at zero frequency of the circuit used for the fitting of the experimental data, i.e. calculating the equivalent resistance of the circuit considering all capacitor as open circuits and all inductors as short-circuits). In order to convert the value of the zero frequency resistance into a corrosion rate, they used anodic and cathodic Tafel coefficient obtained from the literature. For the Tafel coefficients they selected, they found that it was necessary to account for the inductive behaviour in order to obtain correct values of corrosion rate.

The purpose of the present work is to provide further advances in the understanding of the relationship between the electrochemical response and the corrosion phenomena on the magnesium surface. In order to evaluate the electrical response within potential ranges representative of those probed during impedance measurements, the potentiodynamic polarization behaviour in proximity of the free corrosion potential was investigated. Subsequently, a series of impedance measurement were undertaken during free corrosion whilst monitoring in real time the amount of hydrogen evolved from the corroding electrodes, to obtain instantaneous values of corrosion current. As a result, the correlation between the values of resistance obtained from impedance spectroscopy and the corrosion currents measured by hydrogen evolution could be disclosed by direct measurements. Finally, a model accounting for the DC and AC electrical response of a corroding magnesium electrode is presented.

2. Experimental

Magnesium electrodes were obtained from a cast ingot of pure magnesium (nominal composition 99.95 wt.% Mg, composition measured by optical emission spectroscopy: Zn: 0.003, Al: 0.006, Si: 0.005, Mn: 0.006, Fe: 0.003, Ca: 0.005, Pb: 0.001, Pr: 0.010, Nd: 0.010, wt/wt %) and cut into 1 cm^2 (for impedance measurements) or 2 cm^2 (for potentiodynamic polarization measurements) specimens. The magnesium specimens were connected to a copper wire and embedded in epoxy resin, such as the copper was not exposed to the test electrolyte. After polymerization of the resin, the electrodes were mechanically polished with silicon carbide paper

of decreasing size, up to 4000 grit, in order to expose a fresh magnesium surface to the electrolyte.

In order to monitor the hydrogen evolution in real-time and obtain the time-evolution of the corrosion current, the apparatus schematically represented in Fig. 1a, and described in detail in [17] was used. A plastic cylinder, connected by a holder to the plate of a laboratory balance, was completely submerged in the test electrolyte and used to collect the hydrogen evolved from the corroding magnesium surface. The submerged cylinder was initially filled with electrolyte. Progressively, the hydrogen evolved from the magnesium electrode replaced the electrolyte within the submerged cylinder. As a result of the hydrostatic force due to the displacement of the electrolyte within the submerged container, a change in weight was recorded by the balance. From the time evolution of the hydrostatic force, the time evolution of the amount of hydrogen evolved could be calculated and, by Faraday's law, it was converted to the time evolution of the electrical charge associated to hydrogen evolution. Finally, by deriving the charge with respect to the time, the time evolution of the corrosion current was obtained. When two electrodes were used, the value of corrosion current estimated by hydrogen evolution was normalized by the area of both electrodes.

Simultaneously to electrochemical and hydrogen evolution measurements, the surface appearance of the corroding electrodes was recorded (Fig. 1b) by using a computer controlled microscope. In order to evaluate the area of the electrode surface that had undergone corrosion, the acquired images were binarized and the area of the corroded regions computed with an in-house developed Labview program. An example of a corroded surface and corresponding binary image is provided in Fig. 1b and c respectively.

Potentiodynamic polarizations were performed employing the usual 3 electrodes cell configuration at a sweep rate of 1 mV s^{-1}, with the magnesium specimen as working electrode, a commercial calomel electrode as reference electrode and a platinum foil as counter electrode, by using an Iviumstat potentiostat. In order to synchronize hydrogen measurement, image acquisition and potential-time history, the potential of the working electrode was also recorded by a multichannel analogue to digital converter (NI USB-6009), controlled by the same in-house developed Labview program that was used to control the recording of images and weight.

After preliminary testing, it was decided to perform impedance measurement by using a 'modified' two-electrode cell configuration. In practice, two nominally identical magnesium electrodes were connected to individual insulated copper wire and embedded together in a single mould by epoxy resin (Fig. 1b). After polymerization and mechanical polishing, one of the two electrodes was connected to the Working and Reference 2 cables from the potentiostat, while the other electrode was connected to the Counter and Reference 1 cables. Thus, if considering only the electrical circuit comprising the potentiostat, the impedance was performed in a two-electrode cell configuration, where each of the two electrodes acted simultaneously as working electrode and as counter electrode for the other. However, in order to enable synchronization between hydrogen collection and imaging of the surface and electrochemical measurement, a calomel reference electrode was added into the cell and the potential of each individual magnesium electrode was recorded by the NI USB-6009 controlled by the same software that acquired the electrode images and the hydrogen weight. Thus, although the EIS measurement was performed in a 2 electrode configuration, a third reference electrode was placed in the cell and the potential of each individual electrode was recorded. The two-electrode configuration for impedance measurement was preferred to the more traditional 3 electrodes configuration in order to ensure that the amount of hydrogen collected was directly proportional to the metal oxidized. If hydrogen is collected only from one magnesium working electrode (and not from the counter electrode), during the cathodic half-cycle, the hydrogen evolved from the magnesium working electrode surface does not directly correlate with the amount of magnesium oxidized, because the anodic reaction occurs on the counter electrode. By using a two identical electrodes configuration for the impedance measurement, and by collecting the hydrogen from both magnesium electrodes, it is immediately evident that the cathodic current on one electrode (resulting in hydrogen evolution) is necessarily associated with an identical anodic current on the other electrode (magnesium oxidation). Thus, collecting hydrogen during impedance measurements from both identical magnesium electrodes ensures that the amount hydrogen collected directly correlates with the amount of magnesium oxidized and, hence, with the corrosion rate. Additionally, by using the electrode configuration described, the corrosion potential of the electrode pair is free to vary with time, and therefore performing a series of impedance measurement does not modify the natural evolution of the potential-time transient observed for magnesium in the early stages after immersion. Although stationarity of the corrosion process is theoretically required to for reliable impedance measurement, the direct measurement of corrosion current revealed that stationarity was rarely attained (the corrosion current generally in increased with time). Thus, it was deliberately decided to acquire impedance spectra sequentially (in the frequency range 100 kHz to 5 mHz and with a 10 mV amplitude, regardless that the average potential or the corrosion current had attained a steady value.

3. Results

3.1. Potentiodynamic Polarization

Before considering the response measured during impedance measurements, it is useful to analyse the potentiodynamic polarization response in proximity of the free corrosion potential, for polarizations of the same order of those applied during electrochemical impedance spectroscopy (i.e. 10 mV). It is worth recalling that, immediately after immersion in the aggressive electrolyte, the magnesium surface displays a silvery appearance but, as corrosion initiates, the air-formed oxide/hydroxide layer is progressively converted in a dark layer of corrosion products. The regions of the electrode where the air-formed film has been converted into a dark film of corrosion products are referred to as 'dark regions' in this work (Fig. 1b).

The typical potentiodynamic polarization results obtained in 3.5% NaCl, starting the polarization from the free corrosion potential, are presented in Fig. 2. The designation 'Mostly Silvery' refers to a magnesium electrode that displayed less than 5% of the total surface covered by the dark regions (immersed for approximately 900 s in 3.5% NaCl) at the beginning of the potentiodynamic polarization, whereas the designation 'Dark' indicates an electrode that has been immersed in the electrolyte for sufficiently long time (or anodically polarized) such as its surface appeared completely covered by dark corrosion products.

From Fig. 2a, it is evident that the completely black electrode displayed a relatively well-defined linear relationship, with polarization resistance in the region of 22–25 $\Omega\,cm^2$, since the anodic and cathodic polarization curves had similar slopes. Conversely, for a mostly silvery electrode, the anodic behaviour was different from the cathodic behaviour, with the absolute value of current increasing more markedly for a given value of anodic polarization that for the same value of cathodic polarization. Consequently, the terms 'anodic polarization resistance' and 'cathodic polarization resistance' are used here to indicate the

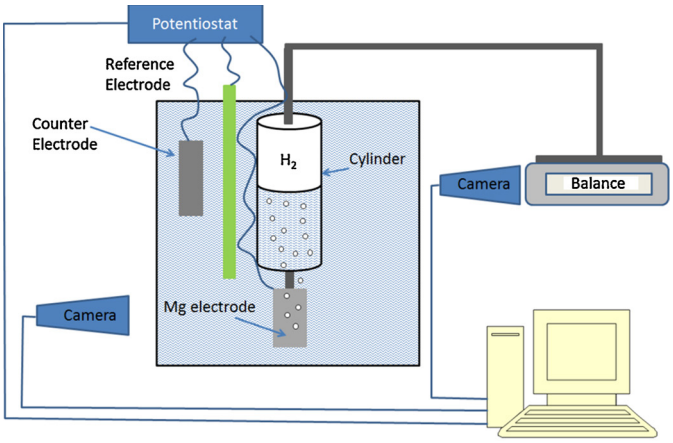

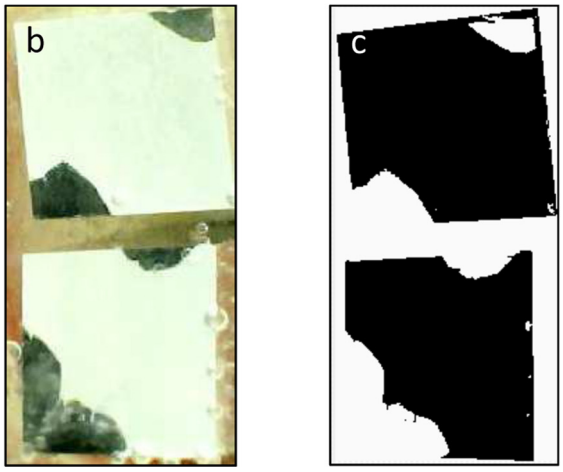

Fig. 1. a) Schematic representation of the setup used to perform electrochemical measurements simultaneously with real-time hydrogen evolution measurement and optical imaging of the corroding magnesium surface [17]. b) Optical image acquired during EIS measurement on two magnesium electrodes and c) image b) after binarization.

reciprocal of the slope of the current density vs. potential curves (in proximity of the corrosion potential) recorded during anodic and cathodic polarization respectively. The mostly silvery electrodes displayed an anodic polarization resistance of 41 $\Omega\,cm^2$, and a cathodic polarization resistance approximately five times higher (221 $\Omega\,cm^2$). The starting point of the cathodic polarization is critical in determining the behaviour in proximity of the corrosion potential. If the potentiodynamic polarization on a completely dark electrode is initiated well below the open circuit potential (Fig. 2b, data from [17]), the asymmetry between the anodic and cathodic behaviour observed for the mostly silvery electrodes is observed also for the completely dark electrode. It should be stressed that such significant deviations from linear behaviour are observed in the same potential range (10 mV above or below the corrosion potential) that is probed during impedance measurements. The overall potentiodynamic polarization behaviour for mostly silvery and dark electrodes is presented in Fig. 2c. It is evident that during anodic polarization, mostly silvery and dark electrodes display similar behaviours, whereas during cathodic polarization, dark electrodes sustain significantly higher currents.

In order to gain further insight, the behaviour during a series of cathodic polarizations separated by 1 h 30 min of free corrosion a was investigated. The potential-time regime applied to the magnesium electrode immersed in 3.5% NaCl solution is presented in Fig. 3a, with the corresponding time evolution of the area fraction of the electrode covered by dark regions, presented in

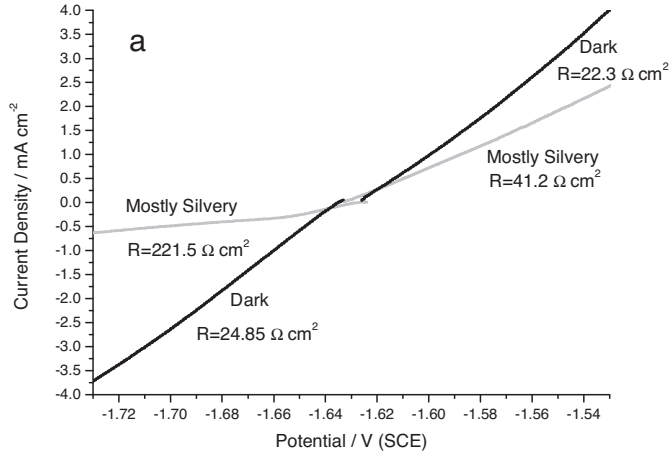

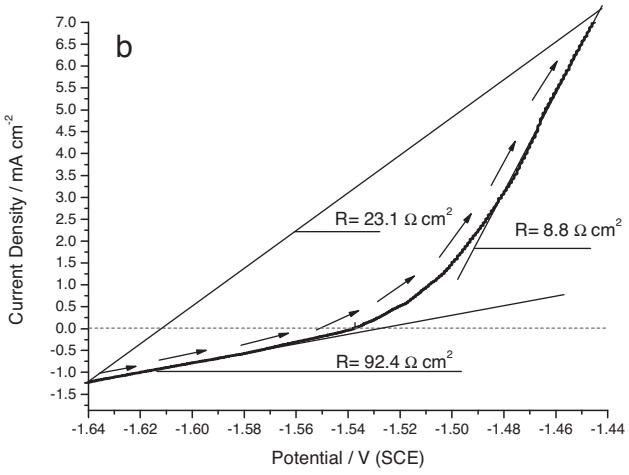

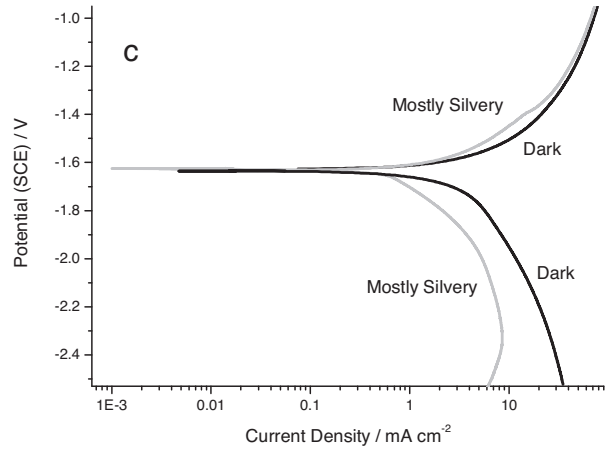

Fig. 2. a) Anodic and cathodic potentiodynamic responses of mostly silvery and completely dark magnesium electrodes in proximity of the corrosion potential measured starting the polarizations at the corrosion potential. b) Potentiodynamic response of a completely dark magnesium electrode measured starting the polarization at −2.2 V vs. SCE. c) Potentiodynamic response of mostly silvery and completely dark magnesium electrodes far from the corrosion potential, starting the polarizations at the corrosion potential (data from [17]).

Fig. 3b. For comparison, the time evolution of the area fraction of the electrode covered by dark regions for a freely-corroding electrode is presented. In Fig. 3c, the optical images acquired during the experiment of Fig. 3a, and used to estimate the time evolution of the area of the dark regions are reported. Each of the

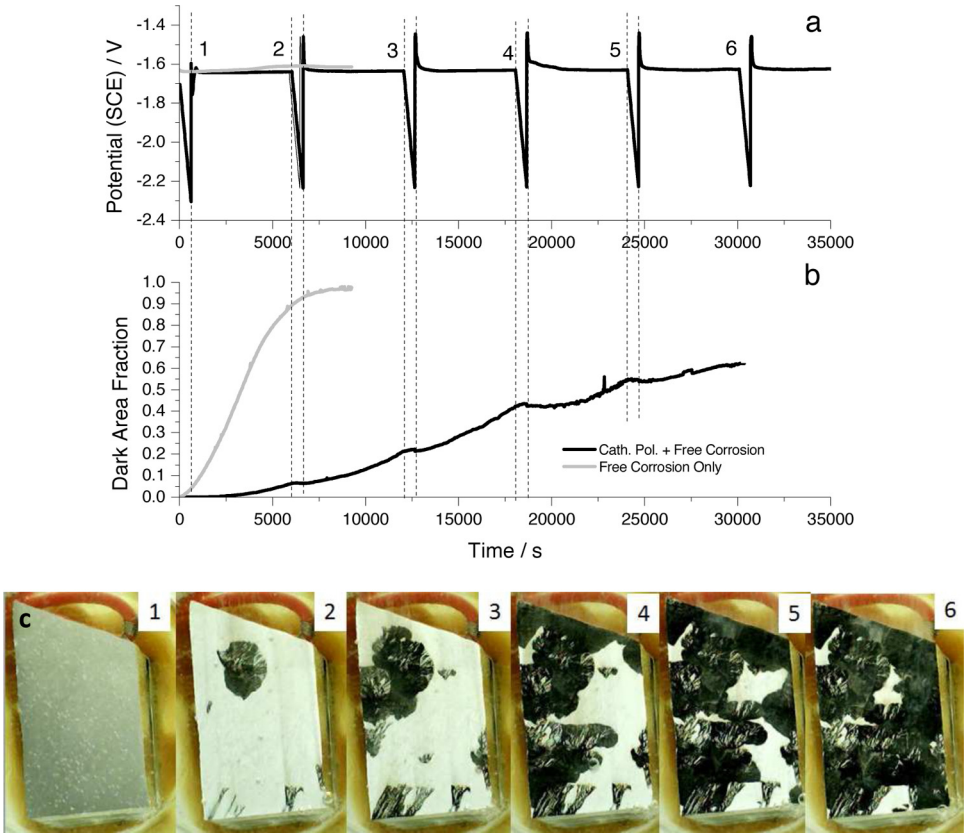

Fig. 3. a) Potential/time regime applied to a magnesium electrode immersed in 3.5% NaCl comprising a series of cathodic potentiodynamic polarizations separated by free corrosion 1.5 h. b) corresponding time evolution of the area of the electrode covered by dark regions during the (for comparison the time evolution of a free corroding electrode is reported from [17]. c) Optical images of the corroding surface during the measurement of Fig. 3a. Numbers on the images correspond to the number of cathodic polarization.

presented images was acquired before the corresponding cathodic polarization. It is immediately observed that the propagation of the dark regions was substantially delayed compared to the freely-corroding case by the repeated application of cathodic polarization. Further, corrosion only propagated during the stage of free corrosion, while during cathodic polarization only abundant hydrogen evolution was observed. Interestingly, it was noted that, after cathodic polarization, corrosion did not propagate from the previously active propagation front, but re-initiated at a new locations (Fig. 3c).

Fig. 4 presents the electrochemical response measured during the series of cathodic polarizations of Fig. 3a. In Fig. 4a, the cathodic response is plotted in linear scale, for variations of potential similar to those experienced during electrochemical impedance spectroscopy. For clarity, the curves have been arbitrarily translated on the potential axis. It is evident that a significant change in the slope of the cathodic polarization curves was observed within the first 2–6 mV below the free corrosion potential. Generally, two regimes were found during cathodic polarization; a first regime, close to the corrosion potential displayed comparatively low apparent cathodic polarization resistance, and a second regime, for larger polarizations, with comparatively higher apparent cathodic polarization resistance. The difference between the first and the second regime in terms of apparent resistance decreased as the corrosion process progressed and the area of the dark regions on the electrode surface increased. Examination of selected cathodic potentiodynamic curves plotted in logarithmic scale (Fig. 4b) provides further insight. With the progression of the corrosion process, the curves shifted towards higher current densities, but displayed similar cathodic Tafel coefficients of about 0.331 V. The values of the cathodic Tafel coefficients measured here in good agreement with the literature [21,23].

3.2. Electrochemical impedance spectroscopy

Electrochemical impedance spectroscopy, coupled with real time hydrogen evolution measurements was performed in order to gain further insight into the correlation between electrochemical measurements and corrosion rates. The experiments were performed by using two nominally identical magnesium electrodes mounted in resin as described previously. Fig. 5 presents the time evolution of a) the individual electrodes potential, b) the corrosion current measured by the hydrogen collection method and c) the fraction of the electrode surface covered by dark regions. In order to evaluate the values of corrosion current associated with each impedance measurement, the value of corrosion current obtained from hydrogen evolution measurement at the time corresponding to the end of each impedance measurement was taken. The procedure is graphically illustrated by the dashed lines in Fig. 5.

The corrosion current measured by hydrogen evolution for nominally identical experimental conditions displayed relatively large variations. Fig. 6 presents the time evolution of the corrosion current for three repeated hydrogen–EIS measurements 3.5% NaCl and two repeated hydrogen–EIS measurements in 0.35% NaCl. The observed variations in the current-time behaviour are attributed to the statistical nature of the corrosion process and to the relatively small electrode size. On a small electrode, the propagation of an active corrosion site could be interrupted by resin at the edges.

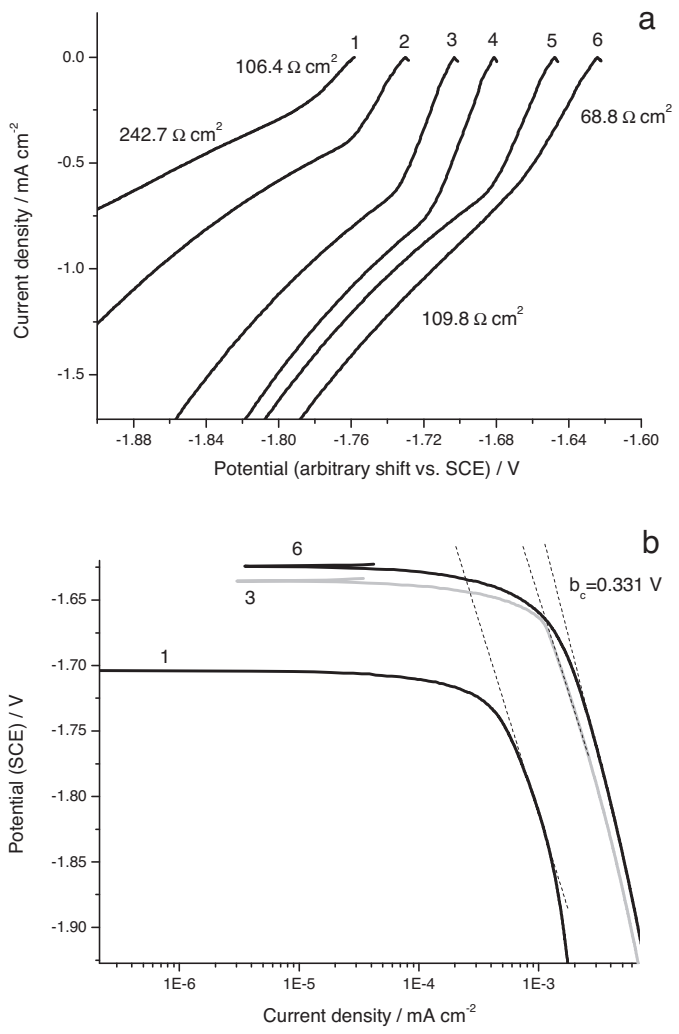

Fig. 4. Cathodic potentiodynamic polarization responses measured during the experiment of Fig. 3. a) Response in proximity of the corrosion potential (linear current scale), translated arbitrarily on the potential axis to improve readability. OCP values for curves 1–6: −1.703 (1), −1.639 (2), −1.636 (3), −1.632 (4), −1.629 (5) and −1.625 (6) V vs. SCE. b) Response for large cathodic polarizations (logarithmic current scale). The numbers on the curves correspond to the number of cathodic polarization in Fig. 3a.

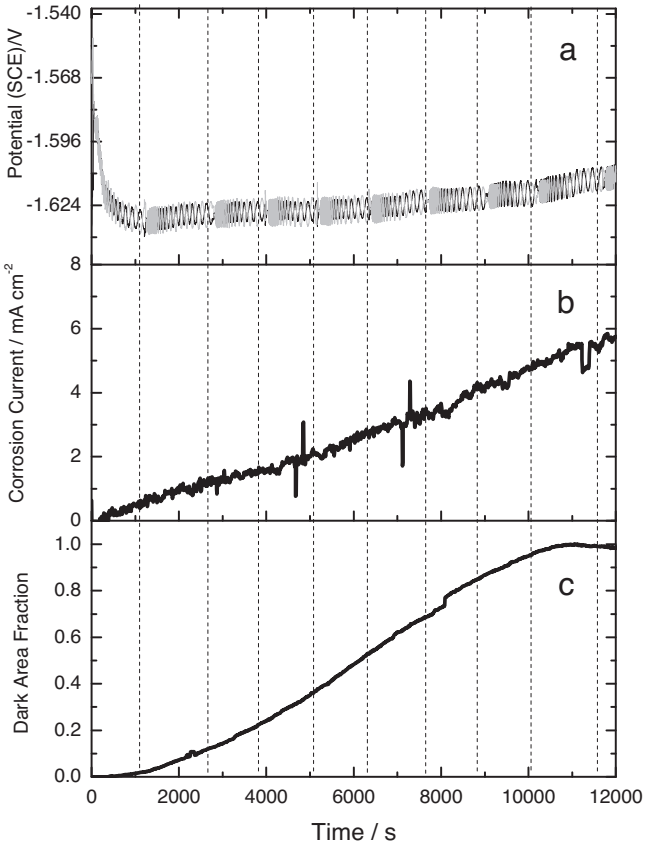

Fig. 5. a) Time evolution of the electrode potentials during a sequence of impedance measurement performed by using the 'modified' two electrode cell configuration in 3.5% NaCl. Corresponding time evolution of b) the corrosion current estimated by real-time hydrogen measurement and c) the fraction of the electrode area covered by dark regions.

Consequently, the location where corrosion initiated and the direction of propagation (which are both random) can have a relatively large effect on the overall corrosion rate, depending on whether the corrosion front is free to propagate or it is stopped by the resin at the edge of the electrode and corrosion is forced to initiate at a new location. As a result of the variations in the current-time behaviour, significant variations in the values of impedance measured under similar conditions were observed. However, the general appearance of the impedance spectra was similar. Typical time series of impedance spectra recorded for high and low concentration of sodium chloride are presented in Fig. 7a and b respectively.

At high frequency, the solution resistance effects dominated, at medium-high frequencies a region of mainly capacitive behaviour, followed by a medium frequency plateau was observed. As expected, the solution resistance was higher in the less concentrated electrolyte. At low frequencies, a reduction in impedance modulus and a corresponding positive phase shift, associated to the inductive behaviour, was revealed. Generally, with increasing immersion time, the modulus of the impedance decreased. The inductive behaviour at the low-frequency end of the spectra was more visible for the measurement performed in the more concentrated NaCl solution.

The impedance spectra were fitted with the circuit, proposed in [21] and reported in Fig. 8a, in order to extract the values of resistances that could be used to estimate the corrosion rate. As discussed in more detail later, C_{ox} and C_{dl} account for the

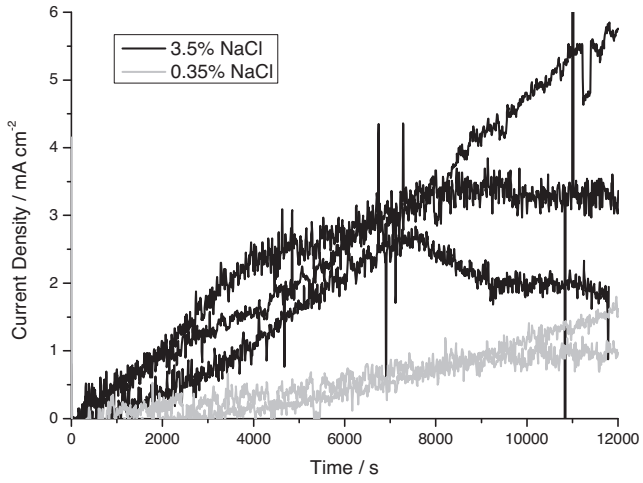

Fig. 6. Time evolution of the corrosion current obtained from real-time hydrogen measurement during repeated EIS measurement in 3.5% and 0.35% NaCl.

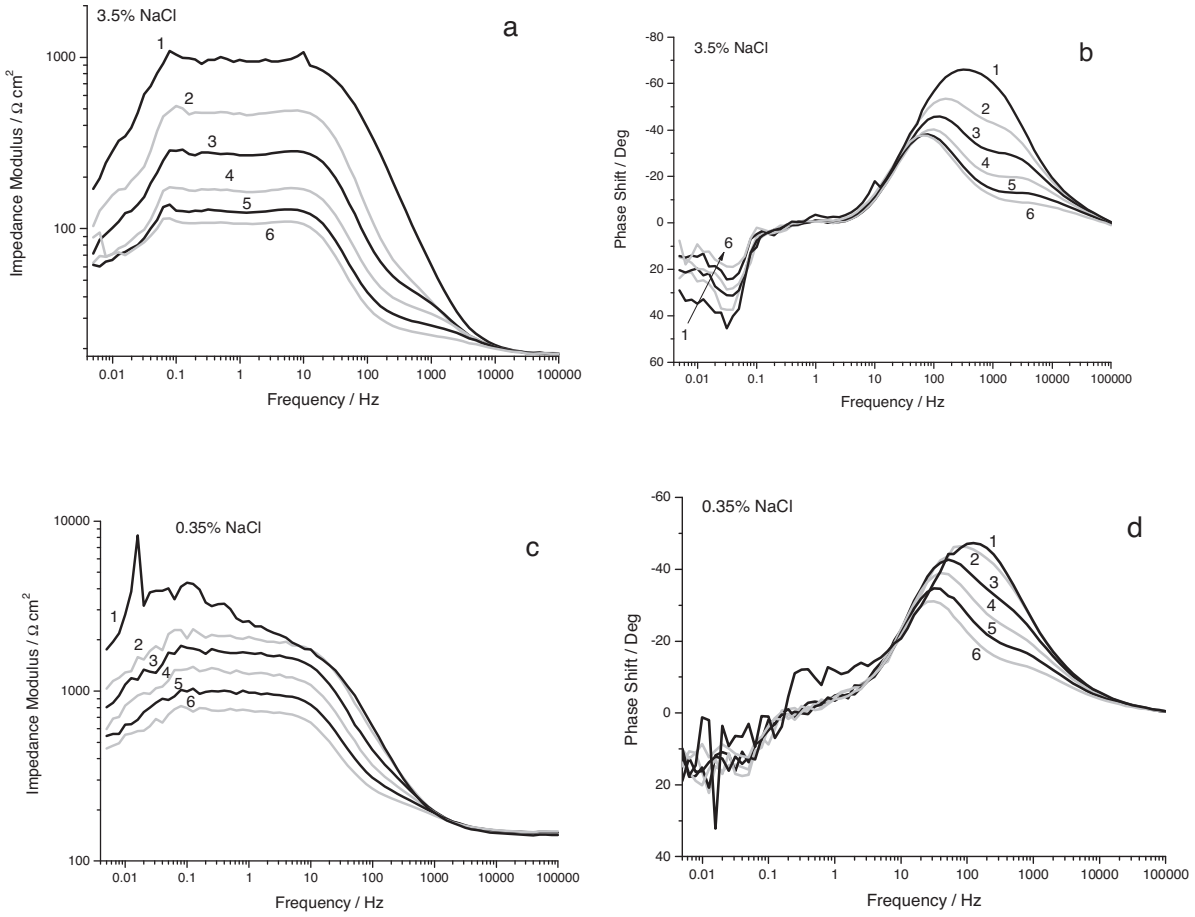

Fig. 7. Typical sequence of impedance modulus (a,c) and phase (b,d) spectra measured in 3.5% (a,b) and 0.35% (c,d) NaCl. The spectra were acquired sequentially and are labelled from 1 (first spectrum acquired) to 6 (last spectrum acquired).

capacitance of oxide/hydroxide layers and charge separation at the locations where hydrogen evolution takes place. R_a and R_{cp} represent the resistances associated to local environmental changes (precipitation of gels, presence of bubbles) nearby the anodic and cathodic regions. Finally, L_a accounts for the variation of the extension of active anodic regions during the sinusoidal polarization and R_{CT} accounts for the charge transfer resistance associated to the reaction of hydrogen evolution. Typical fitting results are compared to the experimental data in Fig. 8b and c. Generally, the simulated and experimental impedance spectra were closely similar, except for the first spectrum of the series where some significant discrepancies between the simulated and the experimental spectrum were occasionally observed. This is likely to be the consequence of the rapid evolution of the magnesium surface during the early stages of immersion, resulting in a corroding system that is far from being stationary. Tables 1 and 2 present the numerical results of the fitting procedure. Fig. 9 illustrates the relationship between the corrosion current directly measured by hydrogen evolution and the reciprocal of a) the zero-frequency resistance (R_A in parallel with the series of R_{CP} and R_{CT}), b) the series of R_{CP} and R_{CT} and c) R_{CT} alone. It is evident that a linear relationship between corrosion current and reciprocal of the resistance was observed, for all the three resistance values. The points representing the experimental data, however, appeared more scattered when the zero-frequency resistance was considered, compared to the case when the charge transfer resistance alone (R_{CT}) or the series between charge transfer (R_{CT}) and corrosion product (R_{CP}) resistance were used. It should be stressed that, even if the time evolution of the corrosion current and impedance spectra recorded under nominally identical conditionswas not well reproducible, the reciprocal of the resistance and the corrosion current were linearly correlated for all the experimental points. This observation suggests that the lack of reproducibility in the corrosion current is due to statistical variation in the corrosion process but the combined measurement of corrosion rate by impedance spectroscopy and hydrogen evolution is reliable.

It is also important to emphasize that, regardless of the underlying kinetic of the electrochemical processes, a linear relationship between corrosion current and reciprocal of resistance is directly observed. Thus, although the potentiodynamic results indicate that the system does not follow a Tafel-type behaviour, the plots of Fig. 9 enable to extract directly values of 'apparent' Stern–Geary coefficient by considering that

$$i_{corr} = \frac{B}{R} \tag{1}$$

Where i_{corr} is the corrosion current density, B is the 'apparent' Stern–Geary coefficient, and R is the value of resistance obtained from fitting of the EIS spectra. Consequently, the apparent Stern–Geary coefficient can be directly estimated from the graphs of Fig. 9, by considering the slope of the fitting lines

$$B = \frac{i_{corr}}{R^{-1}} \tag{2}$$

Clearly, depending on the resistance selected for the calculation, the 'apparent' Stern–Geary coefficient is different; for the

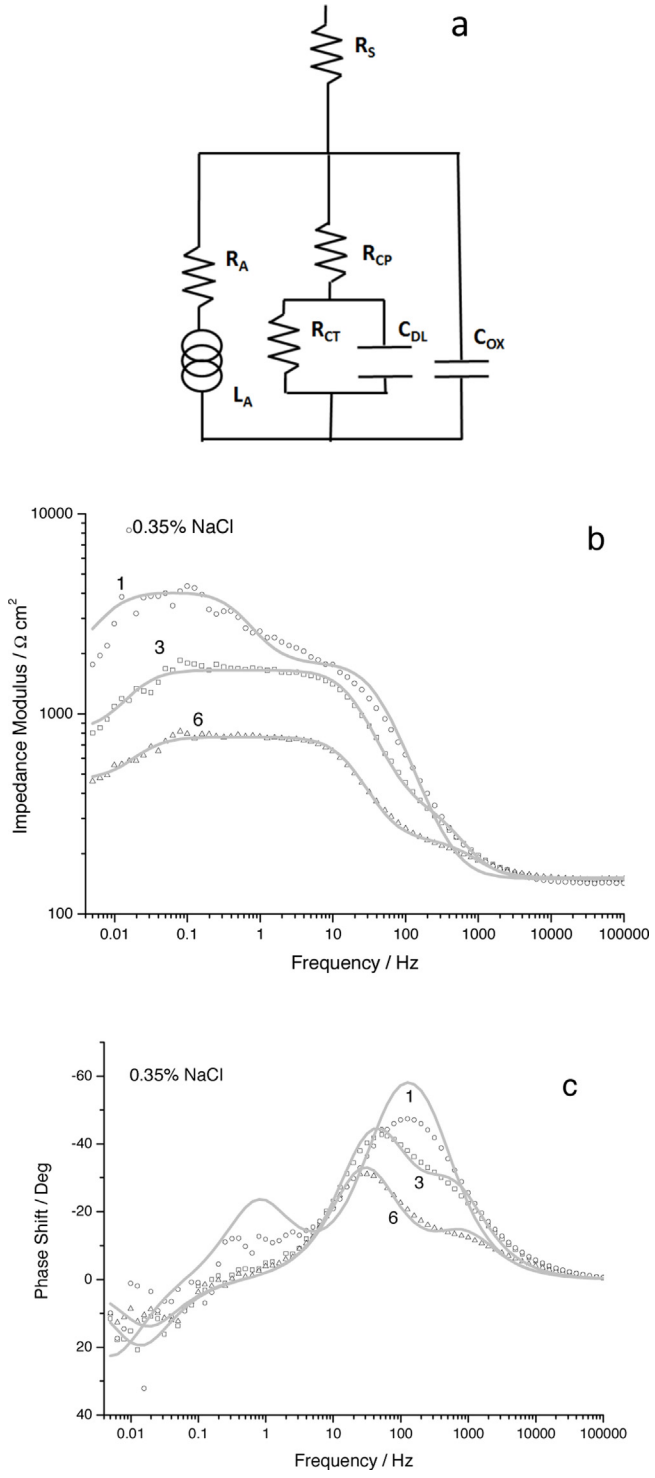

Fig. 8. a) Equivalent circuit used for the fitting of the EIS data. Comparison between calculated and measured impedance modulus b) and phase c) spectra.

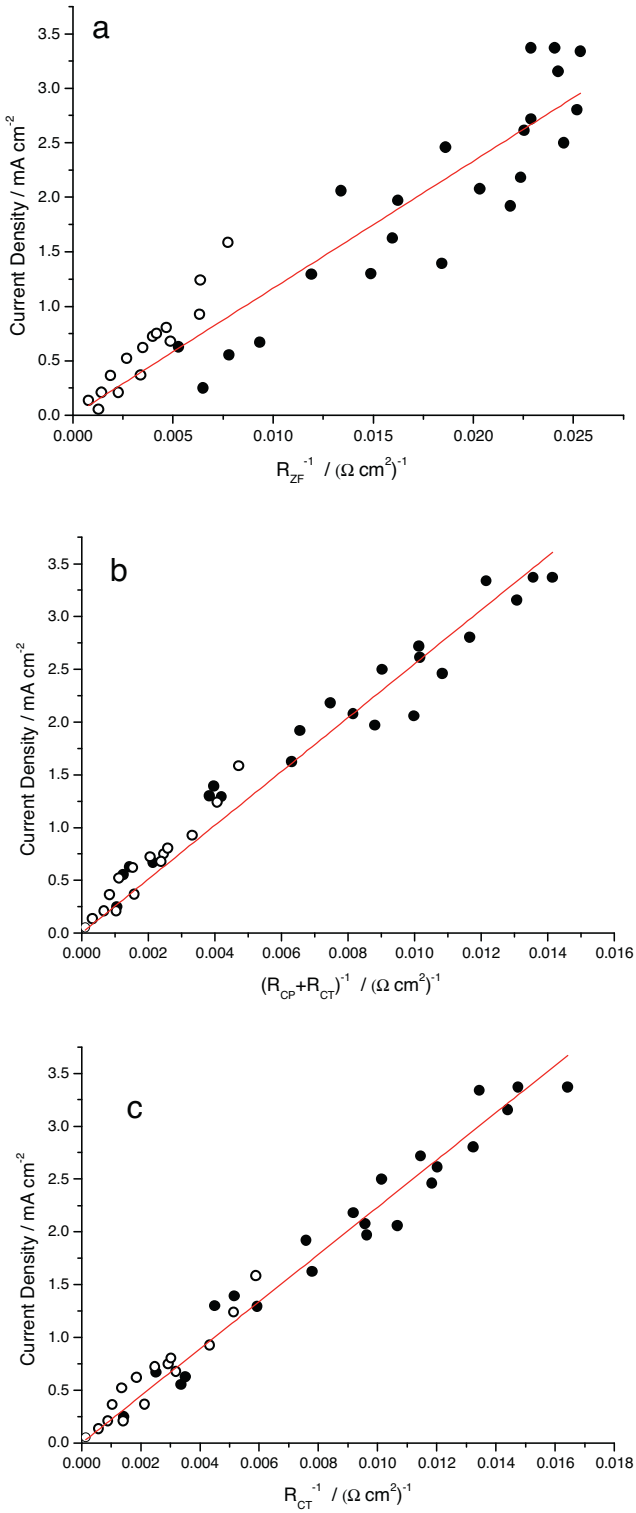

Fig. 9. a) Corrosion current as a function of a) the reciprocal of the zero-frequency resistance (R_A in parallel with the series of R_{CP} and R_{CT}), b) the reciprocal of the series of R_{CP} and R_{CT} and c) the reciprocal of the series of R_{CT}. The slope of the fitting line provides direct estimation of the 'apparent' Stern–Geary coefficients. Filled symbols are obtained from measurement 3.5% NaCl, empty symbols from measurement in 0.35% NaCl.

zero-frequency impedance (R_A in parallel with the series of R_{CP} and R_{CT}) the apparent Stern–Geary coefficient was 116 mV, for the series between the charge transfer resistance and the corrosion product resistance it was 255 mV and for the charge transfer resistance alone it was 223 mV.

Fig. 10 presents the correlation between the area fraction covered by the dark regions and the sum of the oxide capacitance and the double-layer capacitance ($C_{OX}+C_{DL}$). Although the estimation of the area fraction is not as precise as the hydrogen evolution measurement, and the data points appear significantly more scattered compared to the previous datasets, a linear correlation between capacitance and area fraction is observed.

Table 1
Fitting results for the EIS measurements performed in 3.5% NaCl and corrosion current densities obtained from simultaneous measurement of hydrogen evolution.

Measure #	R_S $\Omega\,cm^2$	C_{OX} $\mu F\,cm^{-2}$	L_A $\Omega\,s\,cm^2$	R_A $\Omega\,cm^2$	R_{CP} $\Omega\,cm^2$	C_{DL} $\mu F\,cm^{-2}$	R_{CT} $\Omega\,cm^2$	I_{corr} $mA\,cm^{-2}$
1	15.5	3.06	4420	153	502	7.84	297	0.56
2	16.3	2.50	1830	69.1	58.0	8.29	194	1.39
3	16.5	3.02	1370	67.1	24.9	21.3	109	2.18
4	16.6	3.77	1440	80.8	15.1	34.0	83.2	2.61
5	16.7	4.86	1560	73.9	10.2	41.4	75.5	2.80
6	16.6	6.94	1680	89.5	7.06	45.7	69.4	3.16
7	16.7	14.5	1970	95.1	5.95	43.1	67.8	3.37
8	16.6	29.3	3510	114	9.81	36.0	60.9	3.37
1	19.1	2.60	7170	184	241	2.20	705	0.25
2	19.3	2.68	3840	139	69.7	5.99	398	0.67
3	19.1	2.99	2380	90.5	38.2	12.7	223	1.30
4	18.8	3.49	1510	65.3	20.7	24.7	132	1.92
5	18.9	4.43	1420	64.4	12.1	38.4	98.6	2.50
6	18.8	6.74	1800	129	7.83	49.0	84.4	2.46
7	18.9	11.7	9270	293	6.45	51.5	93.7	2.06
8	19.2	25.0	12600	135	9.67	44	104	1.97
1	17.5	3.18	2830	261	412	12.3	286	0.63
2	17.7	2.84	1260	130	69.7	8.32	169	1.29
3	18.0	3.52	1170	104	30.1	17.2	128	1.63
4	17.7	4.32	1040	82.1	18.1	23.6	104	2.08
5	17.7	5.92	878	78.4	11.3	29.7	87.3	2.72
6	17.7	9.52	824	75.7	7.88	35.2	74.4	3.34

Table 2
Fitting results for the EIS measurement performed in 0.35% NaCl and corrosion current densities obtained from simultaneous measurement of hydrogen evolution.

0.35% NaCl								
Measure #	R_S $\Omega\,cm^2$	C_{OX} $\mu F\,cm^{-2}$	L_A $\Omega\,s\,cm^2$	R_A $\Omega\,cm^2$	R_{CP} $\Omega\,cm^2$	C_{DL} $\mu F\,cm^{-2}$	R_{CT} $\Omega\,cm^2$	I_{corr} $mA\,cm^{-2}$
1	118	3.23	98700	2250	1324	172	1750	0.14
2	118	2.19	19200	1320	379	4.54	1120	0.21
3	118	2.25	15700	968	229	6.76	961	0.37
4	118	2.39	10300	637	153	9.84	739	0.52
5	119	2.64	7710	514	111	14.6	539	0.62
6	120	3.09	622	519	80.8	21.3	405	0.72
7	118	3.91	8630	585	63.0	30.0	342	0.75
8	118	4.42	11800	480	56.5	35.7	331	0.81
1	109	3.24	264100	2960	1390	546.0	1650	na
2	113	2.73	19800	861	1730	2430	7080	0.05
3	109	2.11	14500	813	252	6.96	713	0.21
4	110	2.47	13500	558	161	11.8	470	0.37
5	109	2.87	8510	403	106	17.9	313	0.68
6	109	3.60	9540	334	69.8	26.7	231	0.93
7	109	4.66	12500	436	51.0	33.7	195	1.24
8	110	5.95	15100	331	41.9	39.6	170	1.59

4. Discussion

The potentiodynamic polarization measurements performed within a potential range similar to that used to acquire impedance spectra indicate that corroding magnesium electrodes display a complex behaviour even for very small polarizations above or below the free corrosion potential. In particular, the slope of the anodic polarization curve is, in most cases, significantly different form the slope of the cathodic polarization curve, as evident from Fig. 2. Additionally, close scrutiny of the cathodic polarization behaviour, indicates that a variation in the slope of the curves is observed within the first few millivolt of cathodic polarization, with the apparent resistance being lower for small value of polarization (2–6 mV) and higher for larger values of polarization. These variations in apparent resistance over the potential window used for EIS indicate that the estimation of a zero-frequency value of impedance from fitting of impedance data is of little fundamental interest. In other words a single value of zero-frequency resistance is not capable of reproducing the complex behaviour of the magnesium electrode in proximity of the corrosion potential.

From a practical viewpoint, however, the correlation between the measured impedance spectra and the corrosion rate is of interest, since electrochemical impedance spectroscopy is a relatively non-destructive electrochemical test that can be used to investigate in real-time the corrosion rate. From the presented results, it is evident that there is a good correlation between the values of resistance estimated from EIS and the corrosion rate. Furthermore, the direct measurement of the corrosion current simultaneously with the impedance measurement enables to determine directly the proportionality coefficient that links the corrosion current with the various resistances estimated from EIS. It is found that, if the zero-frequency resistance is used, the points appear comparatively more scattered and the apparent Stern–Geary coefficient is significantly lower (approximately a factor of 2) compared to when the values of the R_{CP} in series with R_{CT} or R_{CT} resistance alone are used.

Based on this experimental observation, it is necessary to speculate on the physical meaning of the apparent Stern–Geary coefficient, and of the Tafel coefficient of magnesium. The Stern–Geary coefficient is given by

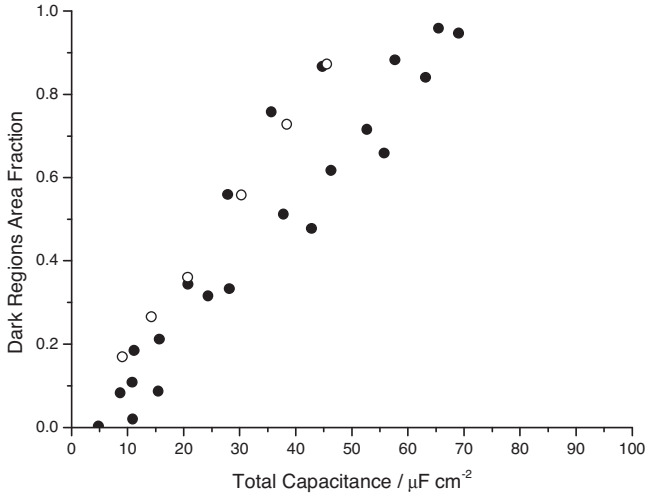

Fig. 10. Fraction of the electrode surface covered by dark regions as a function of the total capacitance ($C_{DL} + C_{OX}$).

$$B = \frac{b_a b_c}{2.3(b_a + b_c)} \quad (3)$$

Where b_a and b_c are the anodic and cathodic Tafel coefficients respectively. For the case of magnesium, the cathodic Tafel coefficient can be experimentally measured; by performing a cathodic polarization a well-defined linear region in the Evan's diagram is evident (Fig. 4b). The measurement of the anodic coefficient is more difficult since magnesium oxidizes fast under anodic polarization and ohmic drop effects become soon dominant [17]. Such ohmic drop effects can be to some extent corrected during or after the measurement, but the correction is not particularly reliable mainly because the presence of bubbles due to copious hydrogen evolution and the formation of hydroxide and gels in proximity of the anodically polarized electrode due to pH increase. These phenomena might result in values of ohmic drop dependent on the applied potential and possibly on the previous polarization history.

In this work, for the first time, values of apparent Stern–Geary coefficient were directly measured for magnesium, together with the cathodic Tafel coefficient. If the system could be described by a Tafel-type kinetic, in principle it should be possible to determine precisely the anodic Tafel coefficient for magnesium by using Eq. (3) with the experimentally measured values of B and b_c. However this route proves to be unsuccessful since, in order to obtain a value of $B = 116$ mV (the lower among the three coefficient measured) with the measured value of b_c (331 mV), a value of $b_a = 1400$ mV is required. Such a high value of the anodic Tafel coefficient is clearly incorrect, since it would imply that the increase in current is less steep in the anodic direction compared to the cathodic direction. This is not the case either for non-IR drop corrected curves or for IR drop corrected curves (see for example Figure 3 in [21]). For the other values of B experimentally measured in this work, negative values anodic Tafel coefficients are obtained from Eq. (3).

The above considerations are in agreement with the experimental observations during potentiodynamic polarization, disclosing a complex behaviour deviating substantially from linearity even for very small polarizations that cannot therefore be approximated by Tafel-type behaviour. Consequently, attempting to estimate the anodic Tafel coefficient proves unsuccessful. Even though the Stern–Geary coefficient cannot be directly estimated reliably from potentiodynamic polarization curves, however, the impedance response is well correlated to the corrosion rate by an 'apparent' Stern–Geary coefficient. The value of such coefficient depends on which resistances in the fitting circuit are selected. If the zero-frequency resistance is used $B = 116$ mV, if the charge transfer resistance is used $B = 223$ mV, if the series between charge transfer resistance and corrosion product resistance is taken, $B = 253$ mV.

4.1. Electrical model for the corroding magnesium surface.

Based on the experimental evidences gathered, an electrical model describing the electrochemical behaviour of the magnesium surface during corrosion can be proposed. During corrosion, the appearance of the electrode surface changes from silvery to dark as a result of the propagation of corrosion. Similarly to what suggested previously [32] the free corroding magnesium surface can be represented as in Fig. 11a. The schematic illustrates that corrosion propagates towards the silvery region by magnesium oxidation. Thus, the anodic corrosion front proceeds and, as a result of the air-formed film disruption, hydrogen evolution on the freshly exposed metal is possible due to the low corrosion potential. As a result of hydrogen evolution, the pH increases and either magnesium hydroxide precipitates or the oxide/hydroxide film growing directly on the metal surface is stabilized. Regardless of the exact nature of the process involved, close to the corrosion front, the corrosion product layer must be relatively thin and, consequently, hydrogen evolution is abundant. Generally, substantially more intense hydrogen evolution is observed in proximity of the propagating corrosion front [14,19]. On the other hand, far from the corrosion front, the corrosion product layer is thicker and less hydrogen evolution takes place. As a result, the corrosion front advances and the silvery regions supporting the air formed oxide are progressively converted into dark regions. Thus, there is a stage when the underlying metal is to some extent exposed to the electrolyte (or only partially covered by an oxide/hydroxide layer) because the air-formed film has been disrupted; at this location, hydrogen evolution is favoured. Such hydrogen evolution increases the pH and this promotes the formation of a film that limits hydrogen evolution itself. The alloy composition and the presence of impurities and/or second phase particles might play a role in the modulating the properties of the growing corrosion product layer, but this aspect has not been investigated in detail here.

At the corrosion potential, the processes is controlled by the rate of the cathodic reaction of hydrogen evolution, since corrosion of magnesium is cathodically controlled, as evident from the potentiodynamic polarization curves. Thus, if the corrosion current is steady, the overall area of the anodic region is constant and determined by the cathodic reaction rate; consequently, the rate at which the air-formed film is attacked equals the rate at which the dark oxide advances in the same direction. Given that not all the dark surface equally supports the cathodic reaction (hydrogen bubbles are generally observed in proximity of the propagating corrosion front [14,19]) there is no direct correlation between the total area of the dark regions and the corrosion rate.

When an anodic polarization is applied (Fig. 11b) additional electrons compared to those consumed by the cathodic reaction on the magnesium electrode are taken by the external circuit (or, equivalently, an anodic current is provided). Thus, the area of the anodic region is free to increase and the overall rate of corrosion propagation increases.

During cathodic polarization, electrons are injected into the corroding electrode (or, equivalently, a cathodic current is provided) and the rate of the cathodic reaction of hydrogen evolution increases whereas the rate of the anodic reaction decreases. As a result, the pH in proximity of the regions capable of supporting hydrogen evolution increases and the formation of the

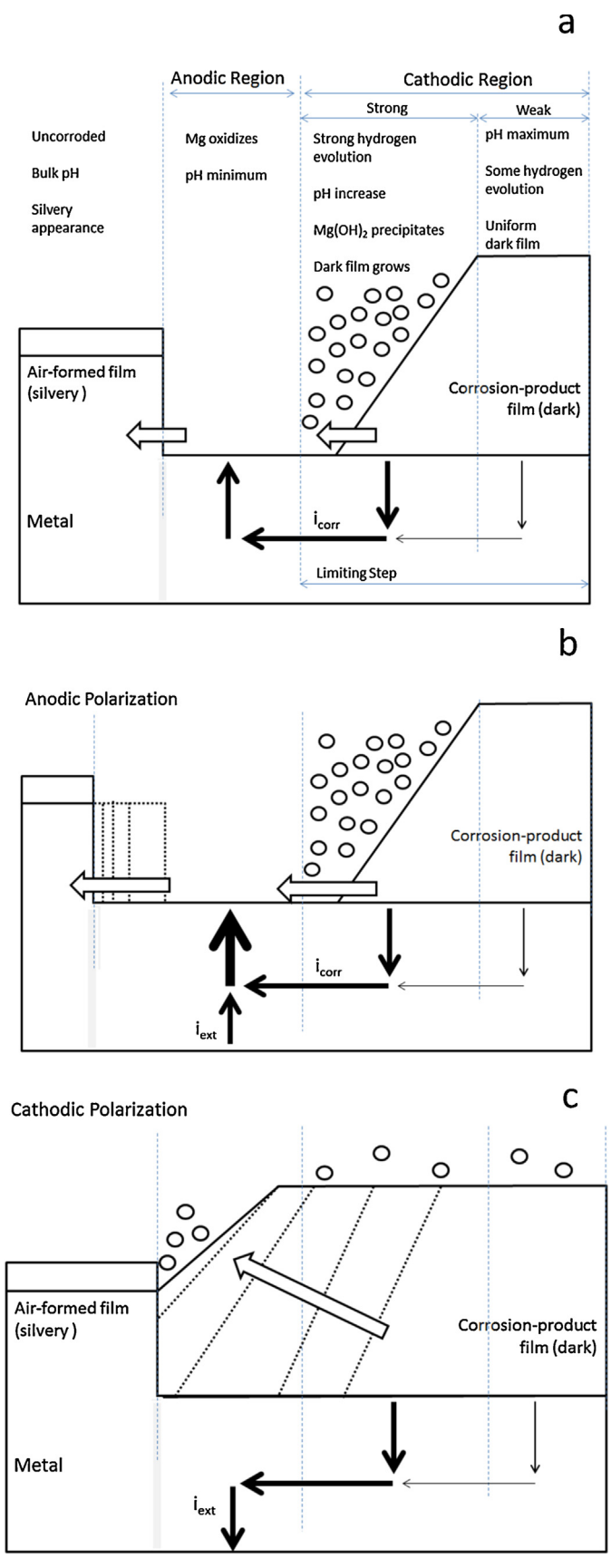

Fig. 11. Qualitative model representing the corroding magnesium surface a) at the corrosion potential, b) during anodic polarization and c) during cathodic polarization.

dark-corrosion products film proceeds faster than the attack of the silvery air-formed oxide. Thus, the area of the anodic region progressively decreases until it becomes negligible and corrosion does not propagate until the cathodic polarization is terminated. The effect of this process can be directly observed by considering the time evolution of the area of the dark regions during a series of cathodic polarizations separated by a period of free corrosion. The propagation of the dark regions does not occur during cathodic polarization (Fig. 3). A further effect of this process is directly observed in the cathodic polarization curves in proximity of the corrosion potential; during the first few millivolt of cathodic polarization the propagation of the regions covered by dark corrosion products takes place at the expenses of the anodic regions. During this stage, the cathodic polarization resistance is comparatively low. Once all the anodic regions have been consumed and the electrode surface is entirely covered either by the residual air-formed film or the relatively thick dark corrosion product layer, hydrogen evolution becomes more difficult and a comparatively higher cathodic polarization resistance is observed. (Fig. 4a)

In the light of the qualitative mechanism proposed, it is possible to relate each element of the equivalent circuit proposed with a specific phenomenon taking place on the electrode surface during impedance measurement or potentiodynamic polarization. In Fig. 12a, the elements of the equivalent circuit are overlapped with the schematic of Fig. 11 (omitting the solution resistance). Two of the three capacitors, C_{AF} and C_{OX} account for the capacitive behaviour of the oxide/hydroxide films (air-formed and corrosion products film, respectively) present on the magnesium surface at any time. The two capacitors are connected in parallel by the electrolyte and by the metal and therefore cannot be distinguished by fitting the impedance data. For this reason, in the equivalent circuit used for the fitting these the two capacitances are grouped together in a single capacitor C_{ox}.

Close to the corrosion front, the cathodic reaction of hydrogen evolution proceeds fast, due to either the absence, the reduced thickness or the non-protective nature of the forming corrosion product film. Across the interface where the cathodic reaction is taking place, charge separation is present at a substantially smaller scale compared to the regions supporting the air-formed film or a stable corrosion product film. In order to account for this, C_{DL} is

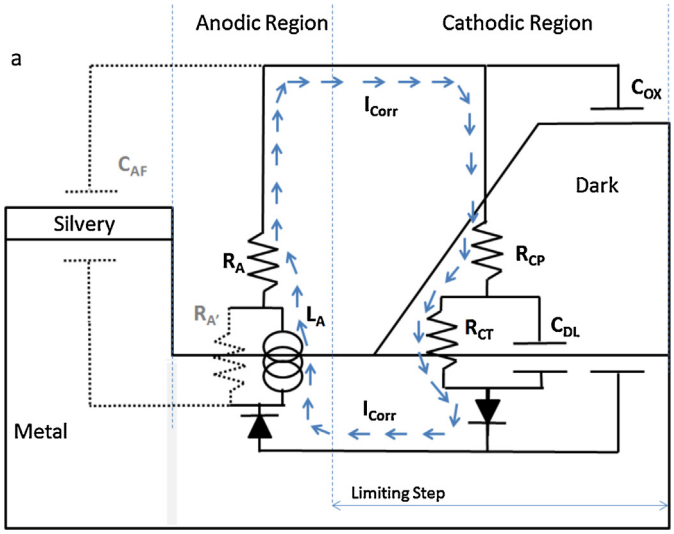

Fig. 12. a) Equivalent circuit overlapped with the model of Fig. 11a, highlighting the physical meaning of the individual components.

present in the equivalent circuit. In parallel with C_{DL}, a charge transfer resistance R_{CT} accounts for the process of electron transfer. As a result of the cathodic reaction, hydrogen (bubbles) and pH increase resulting in the possible precipitation of magnesium oxide/hydroxide gels take place, modifying locally the environment or the oxide properties above the active cathodic sites and a resistor R_{CP} is needed to account for such phenomena. For similar reasons, a resistance R_A is placed in series with the inductor L_A representing the behaviour of the active anodic regions.

The inductive behaviour of the anodic regions deserves further clarification. Qualitatively, the key characteristic of an inductor is that it offers no electrical resistance at zero frequency, while it has infinite resistance at high frequency. However, there is no physical reason to assume that the rate of the anodic reaction should be frequency dependent. Thus, from the physical viewpoint, a resistor $R_{A'}$ must be present, in parallel with the L_A, to account for the fact that the anodic reaction rate cannot decrease to zero during high frequency measurement. Indeed, using a circuit comprising R_A', produces a good fit of the experimental data, but the uncertainty on the values of the other resistances becomes very high. This is due to the fact that the values of R_{CP}, R_{CT}, R_A are in the same order of magnitude and R_A' is short-circuited by L_A at low frequencies while R_{CT} is short-circuited by C_{DL} at high frequencies, and therefore it is difficult to distinguish their effects on the impedance spectra. From the corrosion prospective, however, the presence or absence of R_A' is not a concern, since it is short-circuited by the inductor at low frequency.

In order to understand the nature of the inductance on the corroding magnesium electrode it is useful to consider the behaviour of an ideal inductor. An inductor can be seen as an electrical component that resists to a variation in current by producing a potential difference proportional to the derivative of the current, such as the potential difference across the inductor acts in the direction of opposing the current variation. Thus, increasing the current across an inductor, results in a positive potential. On the other hand, decreasing the current across an inductor, generates a negative potential. The sign of the potential is such as it contrasts the variation in current. If a sinusoidal perturbation is considered, at high frequency, the time derivative of the current is high; therefore the potential produced by the inductor is substantial. Vice versa, at low frequencies, the derivative of the current is low and the potential produced by the inductor is irrelevant.

Such behaviour can be readily translated to the anodic reaction occurring on a corroding magnesium electrode with reference to Figs. 11 and 12. At the corrosion potential, the area of the active anodic regions is limited by the rate of the cathodic reaction and it attains a relatively steady value. When a sinusoidal current perturbation (similar arguments apply for a potential perturbation, but it is easier to consider currents) is applied, the size of the active anodic region tends to increase, to balance the additional current provided by the external circuit (Fig. 11b). If the increase in current is sufficiently slow, the active anodic region can propagate accordingly, and no additional overpotential is needed to sustain the increased current, since the actual current density on the active anodic regions is unchanged, due to propagation. This behaviour is similar to the behaviour of an inductor at zero frequency, i.e. the the current value has no effect on the potential. Generally, however, the propagation (or contraction) of the active anodic region is not instantaneous. As a consequence, a dependence of the potential response on the frequency of the sinusoidal current perturbation is observed. At high frequency, the area of the active anodic region cannot follow the fast current variations and, similarly to the case of the ideal inductor, a large over-potential is needed to accelerate the anodic reaction on the existing active anodic regions (i.e. increasing the current density on the available anodic regions). Again, this behaviour is similar to that of an inductor at high frequency. The diodes in Fig. 12a have been added to account (qualitatively) for the fact that the inductive part of the circuit relates to the anodic reaction and the capacitive part of the circuit relates to the cathodic reaction, and that the corrosion current flows in the direction indicated by the arrows. The presence of the diodes also accounts for the difference in slope of the anodic and cathodic potentiodynamic polarization curves in proximity of the corrosion potential. Additionally, it also accounts for the observation of King et al. [21], who revealed an enhancement of the inductive behaviour when performing EIS on magnesium above the free corrosion potential and a suppression of the inductive behaviour when performing EIS below the free corrosion potential.

The experimental evidences obtained in this work can be interpreted on the basis of the above model. Firstly, the similarity in behaviour observed during anodic polarization for a dark electrode and a silvery electrode are discussed. According to the proposed model, the anodic current directly correlates with the area of the anodic regions which, at the free corrosion potential, is limited by the cathodic reaction; when anodic current is provided through the external circuit, the area of the anodic region adjusts to the external current, regardless of the pre-existing surface condition. As a consequence, the initial state of the surface does not affect substantially the anodic polarization response. The change in slope of the I/V curves in proximity of the free corrosion potential relates to the fact that, unlike for Tafel behaviour, the anodic reaction largely dominates on the cathodic reactions even for small anodic polarizations, due to the fact that the active anodic region rapidly adjusts to the total current available. For polarization in the cathodic direction, the passivation of the active anodic regions occurs rapidly (Fig. 11c) and therefore even a few millivolts below the free corrosion potential the cathodic reaction largely dominates on the anodic reaction. This behaviour is represented by the diodes in Fig. 12.

The change of slope in the cathodic polarization curves (Fig. 3) can be explained similarly. At the free corrosion potential, the electrons generated at active anodic regions are balanced by those consumed at the active cathodic regions. The balance is perturbed by the cathodic polarization that results in increased availability of electrons that ultimately induces excess alkalinisation compared to free corrosion and consequent propagation of the dark corrosion product film (Fig. 11c) faster than the propagation of the corrosion front. During the early stages of cathodic polarization, the propagation of the corrosion product film towards the active anodic regions is possible and the apparent resistance is relatively low. Once all the active anodic regions have been consumed (Fig. 11c) the propagation is no longer possible and the apparent resistance increases (Fig. 3a). This is confirmed by the observation that the dark regions do not propagate during cathodic polarization (Fig. 4c). After the propagation stage is finished, the cathodic reaction on the dark corrosion product film follows Tafel kinetics, possibly due to the fact that the limiting step is the charge transfer across the dark film.

Concerning the interpretation of the correlation between measured corrosion current and resistance values obtained from impedance measurement, the reduced scattering observed when considering the charge transfer and the series between charge transfer and corrosion products resistance (rather than the zero-frequency resistance) is due to the fact that the cathodic reaction provides the limiting step for corrosion propagation. Therefore the corrosion rate is directly proportional to the values of R_{CP} and R_{CT}. Indirectly, the values of R_{CP} and R_{CT} determine the value of R_A, and therefore also the zero frequency resistance correlates well with the corrosion rate. However, due to the less direct dependence, the points in the plots for the determination of the apparent Stern–

Geary coefficient appear more scattered. Based on these considerations, it appears that from the practical viewpoint, the most reliable estimation of the corrosion current from EIS data is likely to be provided considering the series of R_{CP} and R_{CT} (since these two values account for the rate-determining cathodic reaction) and using for the calculations the relevant value of apparent Stern–Geary coefficient ($B = 253$ mV).

5. Summary

The corrosion behaviour of magnesium has been investigated by potentiodynamic polarization and electrochemical impedance spectroscopy. Potentiodynamic polarization revealed significant deviations from linear behaviour in proximity of the corrosion potential, indicating the estimation of the corrosion current by using a Stern–Geary coefficient obtained from potentiodynamic polarization curves is not adequate. However, direct measurement of the corrosion current by hydrogen collection, performed simultaneously with EIS measurements, revealed that the reciprocal of the values of resistance estimated by EIS are linearly correlated with the corrosion current. The experimentally measured proportionality constant provides an 'apparent' Stern–Geary coefficient that can be used to evaluate the corrosion current from EIS data. From the value of the experimentally measured apparent Stern–Geary coefficient and of the cathodic Tafel coefficient, it is not possible to obtain a reliable value for the anodic Tafel coefficient, since magnesium corrosion doesn't follow Tafel's type kinetics.

Based on the behaviour observed during potentiodynamic polarization and on equivalent circuit analysis of EIS spectra, it can be concluded that corrosion proceeds by magnesium oxidation at active anodic regions. Where the air-formed oxide/hydroxide layer is disrupted, hydrogen evolves vigorously, increasing the pH and inducing the precipitation of magnesium hydroxide behind the corrosion front. Once the precipitated film is sufficiently thick, the rate of hydrogen evolution behind the corrosion front decreases. Corrosion proceeds by translation of the active anodic region towards the uncorroded silvery regions, which is followed by propagation of the dark regions. Application of an anodic (or cathodic) polarization results in faster (or slower) propagation of the active anodic region with respect to the propagation dark regions.

Acknowledgements

EPSRC is acknowledged for provision of financial support through the LATEST2 Programme Grant (EP/H020047/1). Prof M. Di Natale is acknowledged for helpful discussions.

References

[1] D. Aurbach, Y. Gofer, Z. Lu, A. Schechter, O. Chusid, H. Gizbar, Y. Cohen, V. Ashkenazi, M. Moshkovich, R. Turgeman, E. Levi, J. Power Sources 97–98 (2001) 28–32.
[2] D. Aurbach, Z. Lu, A. Schechter, Y. Gofer, H. Gizbar, R. Turgeman, Y. Cohen, M. Moshkovich, E. Levi, Nature 407 (2000) 724–727.
[3] D. Aurbach, G.S. Suresh, E. Levi, A. Mitelman, O. Mizrahi, O. Chusid, M. Brunelli, Adv. Mater. 19 (2007) 4260–4267.
[4] M. Andrei, F. Di Gabriele, P.L. Bonora, D. Scantlebury, Mater. Corros. 54 (2003) 5–11.
[5] F. Guadarrama-Muñoz, J. Mendoza-Flores, R. Duran-Romero, J. Genesca, Electrochim. Acta 51 (2006) 1820–1830.
[6] J.G. Kim, S.J. Koo, Corrosion 56 (2000) 380–388.
[7] G.T. Parthiban, T. Parthiban, R. Ravi, V. Saraswathy, N. Palaniswamy, V. Sivan, Corros. Sci. 50 (2008) 3329–3335.
[8] M.P. Staiger, A.M. Pietak, J. Huadmai, G. Dias, Biomaterials 27 (2006) 1728–1734.
[9] F. Witte, Acta Biomaterialia 6 (2010) 1680–1692.
[10] J.H. Nordlien, S. Ono, N. Masuko, K. Nisancioglu, J. Electrochem. Soc. 142 (1995) 3320–3322.
[11] G. Song, A. Atrens, D. St John, X. Wu, J. Nairn, Corros. Sci. 39 (1997) 1981–2004.
[12] R.L. Petty, A.W. Davidson, J. Kleinberg, J. Am. Chem. Soc. 76 (1954) 363–366.
[13] T.R. Thomaz, C.R. Weber, T. Pelegrini, L.F.P. Dick, G. Knörnschild, Corros. Sci. 52 (2010) 2235–2243.
[14] G. Williams, H. Neil McMurray, J. Electrochem. Soc. 155 (2008) C340–C349.
[15] N.T. Kirkland, G. Williams, N. Birbilis, Corros. Sci. 65 (2012) 5–9.
[16] S. Lebouil, A. Duboin, F. Monti, P. Tabeling, P. Volovitch, K. Ogle, Electrochimi. Acta (2013) .
[17] M. Curioni, Electrochim. Acta 120 (2014) 284–292.
[18] G.S. Frankel, A. Samaniego, N. Birbilis, Corros. Sci. 70 (2013) 104–111.
[19] G. Williams, N. Birbilis, H.N. McMurray, Electrochem. Commun. 36 (2013) 1–5.
[20] V. Shkirskiy, A.D. King, O. Gharbi, P. Volovitch, J.R. Scully, K. Ogle, N. Birbilis, ChemPhysChem 16 (2015) 536–539.
[21] A.D. King, N. Birbilis, J.R. Scully, Electrochim. Acta 121 (2014) 394–406.
[22] G. Song, D. StJohn, Journal of Light Metals 2 (2002) 1–16.
[23] F. Cao, Z. Shi, J. Hofstetter, P.J. Uggowitzer, G. Song, M. Liu, A. Atrens, Corros. Sci. 75 (2013) 78–99.
[24] Z. Qiao, Z. Shi, N. Hort, N.I. Zainal Abidin, A. Atrens, Corros. Sci. 61 (2012) 185–207.
[25] M. Taheri, J.R. Kish, N. Birbilis, M. Danaie, E.A. McNally, J.R. McDermid, Electrochim. Acta 116 (2014) 396–403.
[26] J. Janiec-Anwar, G. Thompson, X.R. Zhou, M. Curioni, M. Turski, T. Wilks, Galvanic corrosion between magnesium alloys and steel, Mater. Sci. Forum 765 (2013) 648–652.
[27] A. Pardo, M.C. Merino, A.E. Coy, F. Viejo, R. Arrabal, S. Feliú Jr., Electrochim. Acta 53 (2008) 7890–7902.
[28] G. Baril, G. Galicia, C. Deslouis, N. Pébère, B. Tribollet, V. Vivier, J. Electrochem. Soc. 154 (2007) C108–C113.
[29] A.D. Sudholz, K. Gusieva, X.B. Chen, B.C. Muddle, M.A. Gibson, N. Birbilis, Corros. Sci. 53 (2011) 2277–2282.
[30] A.D. Südholz, N. Birbilis, C.J. Bettles, M.A. Gibson, J. Alloys Compd. 471 (2009) 109–115.
[31] M. Curioni, T. Monetta, F. Bellucci, Corrosion behaviour of magnesium electrodes investigated by real-time hydrogen measurement, Eurocorr 2014, Pisa, Italy, 2014.
[32] G.L. Song, Z. Xu, Corros. Sci. 63 (2012) 100–112.